Journal of Biomechanics xxx (2018) xxx–xxx

Contents lists available at ScienceDirect

Journal of Biomechanics

journal homepage: www.elsevier.com/locate/jbiomech
www.JBiomech.com

Dependence of leukocyte capture on instantaneous pulsatile flow

Umberto Ciri [a], Rita Bhui [b], Jorge Bailon-Cuba [c], Heather N. Hayenga [d], Stefano Leonardi [a,*]

[a] Department of Mechanical Engineering, The University of Texas at Dallas, Richardson, TX, USA
[b] Department of Physics, The University of Texas at Dallas, Richardson, TX, USA
[c] Department of Mechanical Engineering, Polytechnic University of Puerto Rico, San Juan, Puerto Rico
[d] Department of Bioengineering, The University of Texas at Dallas, Richardson, TX, USA

ARTICLE INFO

Article history:
Accepted 30 May 2018
Available online xxxx

Keywords:
Leukocyte capture
Hemodynamics
Time-averaged flow
Instantaneous flow
Direct numerical simulation

ABSTRACT

Atherosclerosis, an artery disease, is currently the leading cause of death in the United States in both men and women. The first step in the development of atherosclerosis involves leukocyte adhesion to the arterial endothelium. It is broadly accepted that blood flow, more specifically wall shear stress (*WSS*), plays an important role in leukocyte capture and subsequent development of an atherosclerotic plaque. What is less known is how instantaneous *WSS*, which can vary by up to 5 Pa over one cardiac cycle, influences leukocyte capture. In this paper we use direct numerical simulations (DNS), performed using an in-house code, to illustrate that leukocyte capture is different whether as a function of instantaneous or time-averaged blood flow. Specifically, a stenotic plaque is modeled using a computational fluid dynamics (CFD) solver through fully three-dimensional Navier-Stokes equations and the immersed boundary method. Pulsatile triphasic inflow is used to simulate the cardiac cycle. The CFD is coupled with an agent-based leukocyte capture model to assess the impact of instantaneous hemodynamics on stenosis growth. The computed wall shear stress agrees well with the results obtained with a commercial software, as well as with theoretical results in the healthy region of the artery. The analysis emphasizes the importance of the instantaneous flow conditions in evaluating the leukocyte rate of capture. That is, the capture rate computed from mean flow field is generally underpredicted compared to the actual rate of capture. Thus, in order to obtain a reliable estimate, the flow unsteadiness during a cardiac cycle should be taken into account.

© 2018 Elsevier Ltd. All rights reserved.

1. Introduction

The prevalence and consequences of Cardiovascular Diseases (CVD) make them one of the world's most prominent diseases. CVD are the primary cause of death in the world with more than 17.3 million deaths per year and the total direct and indirect cost of CVD and stroke in 2016 were more than $316.6 billion. Many CVD develop as a result of atherosclerosis, including coronary heart disease, carotid artery disease (stroke), peripheral artery disease (PAD), and angina (chest pain). As defined by the American Heart Association, atherosclerosis is a condition in which plaque builds up inside the arterial wall. Plaque is made of cholesterol, leukocytes and other arterial cells, fatty substances, cellular waste products, calcium, elastin, collagen, and fibrin. The plaque may partially or completely block the blood's flow through an artery, thus influencing blood hemodynamics. In this paper we show how instantaneous pulsatile flow around a plaque influences leukocyte capture to the arterial wall.

Clinical techniques used to measure flow rates in vivo suggest a positive correlation between the hemodynamics and atherosclerotic growth and remodeling. Gibson et al. (1993) found a significant correlation between vessel low wall shear stress (*WSS*) and increased rate of atherosclerosis progression. They used quantitative angiography to calculate the change in coronary arterial diameter over 3 years. *WSS* was calculated by a finite-element model employing the Navier-Stokes equations and assuming a constant coronary flow rate of 8 ml/s. Similarly, others have used in vitro and in vivo studies to show correlations between the *WSS*, leukocyte infiltration and wall composition. In-vivo, plaque regions with average low *WSS* tend to be or become fibrotic (Chatzizisis et al., 2008). Likewise, in vitro studies show low *WSS* is correlated with a higher rate of leukocyte extravasation (Bailey et al., 2007). Conversely, longitudinal studies suggest plaque regions with an average high *WSS* tend to exhibit regression of fibrotic tissue (Timmins et al., 2015; Samady et al., 2011). In-vitro studies also show high *WSS* regions have little leukocyte extravasation (Burns

* Corresponding author.
E-mail address: stefano.leonardi@utdallas.edu (S. Leonardi).

https://doi.org/10.1016/j.jbiomech.2018.05.044
0021-9290/© 2018 Elsevier Ltd. All rights reserved.

Please cite this article in press as: Ciri, U., et al. Dependence of leukocyte capture on instantaneous pulsatile flow. J. Biomech. (2018), https://doi.org/10.1016/j.jbiomech.2018.05.044

et al., 2007; Sheikh et al., 2003; Barreiro et al., 2005; Cinamon and Alon, 2003). It is broadly accepted *WSS* plays an important role in leukocyte extravasation and plaque remodeling; however, it is less known how the instantaneous wall shear stress, which can vary by up to 5 Pa during one cardiac cycle (Hasan et al., 2013), influences leukocyte transmigration and resulting plaque progression. In this paper we show how leukocyte capture as a function of instantaneous flow is significantly different than as a function of time-averaged flow.

Several numerical studies have illustrated the spatiotemporal dynamics of blood flow within the coronary artery, and were used to inform the model presented herein. Hasan et al. (2013) used a computational fluid dynamics model to investigate the effect of cyclic motion (i.e. bending and stretching) on coronary blood flow. In this study, the artery was modeled as an anisotropic nonlinear elastic material (via the five-parameter Mooney-Rivlin hyperelastic model). Blood was assumed as an incompressible Newtonian fluid and flow was solved using continuity and Navier-Stokes equations. Hasan et al. (2013) concluded the bending motion of the coronary artery has little effect on flow properties (i.e., blood flow velocity, blood shear stress and wall shear stress) but greatly affects the stresses within the artery wall. Since we are modeling leukocyte capture as a function of blood hemodynamics, the model presented herein does not account for wall motion. Chaichana et al. (2012) studied the hemodynamic effect of realistic coronary plaques reconstructed based on high-resolution CT data of human coronary plaques. Computational Fluid Dynamics (CFD) analysis revealed the classic features: *WSS* was highest at the peak stenosis (minimum luminal diameter) and recirculation regions occurred post-stenosis. Even though this study used realistic (i.e. non-axisymmetric) plaque geometries the degree of stenosis was the primary factor giving rise to the observed hemodynamic changes. Therefore, our model uses simplified plaque geometries to keep the focus on the effects of instantaneous versus steady flow on leukocyte capture.

In this paper, a direct numerical simulation (DNS) of pulsatile blood flow in a branch-less circular cylindrical coronary artery is implemented. Incompressible, pulsatile flow of blood as a Newtonian fluid is solved using an in-house parallel code. *WSS* is computed from the transient fully 3D velocity field at the wall. The stenotic wall of the artery is introduced using the immersed boundary method (Orlandi and Leonardi, 2006). Calculated spatiotemporal fields from the DNS are then compared to, and agree well with, those obtained using a commercial program, COMSOL. In the second part of the paper, *WSS* computed from the DNS is coupled with a leukocyte capture model as presented by Bhui and Hayenga (2017). We then compare the total value of leukocyte capture during time-averaged and instantaneous flow. The instantaneous *WSS* plays a critical role in leukocyte capture and thus vascular remodeling of the stenotic artery.

2. Numerical method

We consider an artery as a rigid circular cylinder with a length-to-diameter ratio $L/D = 32$. The Navier-Stokes equations for a Newtonian incompressible fluid are assumed as the governing equations:

$$\nabla \cdot \mathbf{u} = 0 \tag{1}$$

$$\frac{\partial \mathbf{u}}{\partial t} + (\mathbf{u} \cdot \nabla)\mathbf{u} = -\frac{1}{\rho}\nabla p + \nu \nabla^2 \mathbf{u} \tag{2}$$

Here $\mathbf{u}$ is the velocity vector, p the pressure, $\rho = 1060\ \mathrm{kg/m^3}$ is the blood density, $\nu = 3.3 \cdot 10^{-6}\ \mathrm{m^2/s}$ is the blood kinematic viscosity, and t is time. The inlet velocity profile is assumed to be axisymmetric and parabolic:

$$u = 2\,u_{\mathrm{bulk}}(t) \cdot \left[1 - \frac{r^2}{(D/2)^2}\right] \tag{3}$$

where u_{bulk} is the pulsatile bulk velocity, r is the radial distance from the artery axis. The amplitude of the bulk velocity follows the triphasic waveform signal modified from He and Ku (1996) (shown in Fig. 2a). The period is 0.8 s ($T = 0.8$ s), which gives a Womersley number of $\alpha = (D/2)\sqrt{2\pi/(\nu T)} \approx 2.3$.

A Gaussian function is used to model the stenotic region of the arterial wall:

$$r_w(x, \vartheta) = \frac{D}{2} - h \exp\left[-a_1 \left(\frac{x}{D}\right)^2\right] \cdot \exp\left(-a_2 \vartheta^2\right) \tag{4}$$

where x and ϑ are the streamwise and azimuthal coordinates, respectively. The maximum height of stenosis is h, and a_1 and a_2 are the shape parameters. We have considered both axisymmetric and three-dimensional geometries. In the first case, the azimuthal shape parameter, a_2, is set to $a_2 = 0$; for the three-dimensional case, $a_2 = 2.68$. In both cases, the axial shape parameter is kept fixed to $a_1 = 8.41$. To assess the effect of different degrees of flow obstruction, we varied the height of the stenosis. For the axisymmetric geometry, we have considered three cases: $h/D = 0.1, 0.2, 0.3$. Two further simulations with the three-dimensional geometry ($a_2 = 2.68$) have been performed using $h = 0.1D$ and $h = 0.2D$. Fig. 1 illustrates the geometries of the stenotic wall used in this study.

Eqs. (1) and (2) can be non-dimensionalized by appropriately normalizing all the variables by reference values of velocity, length and density. Herein, the mean bulk velocity u_{mean}, the arterial diameter D, and the blood density are the selected reference values. Scaling the variables in (1) and (2) yields the non-dimensional Navier-Stokes equations:

$$\nabla_* \cdot \mathbf{u}_* = 0 \tag{5}$$

$$\frac{\partial \mathbf{u}^*}{\partial t^*} + (\mathbf{u}^* \cdot \nabla_*)\mathbf{u}^* = -\nabla_* p^* + \frac{1}{Re}\nabla_*^2 \mathbf{u}^* \tag{6}$$

where quantities denoted by a superscript $*$ refer to non-dimensional variables:

$$\mathbf{u}^* = \frac{\mathbf{u}}{u_{\mathrm{mean}}}, \qquad t^* = \frac{t u_{\mathrm{mean}}}{D}, \qquad p^* = \frac{p}{\rho u_{\mathrm{mean}}^2}$$

and

$$[\nabla_*]_i = \frac{\partial}{\partial x_i^*} \quad \text{with} \quad x_i^* = \frac{x_i}{D}$$

The non-dimensional momentum Eq. (6) explicitly depends on the Reynolds number. The Reynolds number, based on the artery diameter $D = 2.9$ mm and on the mean bulk velocity u_{mean}, is $Re = u_{\mathrm{mean}} D/\nu \approx 340$, where:

$$u_{\mathrm{mean}} = \frac{1}{T}\int_0^T u_{\mathrm{bulk}}(t)\,\mathrm{d}t = 0.384\ \mathrm{m/s} \tag{7}$$

The in-house numerical code solves the non-dimensional equations. Eqs. (5) and (6) are discretized using a finite differences scheme on a Cartesian grid. The numerical scheme is described in detail in Orlandi (2000). Central finite differences are used for the spatial derivatives, which yield a second-order conservative scheme. Time-advancement is performed with a hybrid third-order low-storage Runge-Kutta scheme with the non-linear terms treated explicitly, and the linear terms implicitly. A fractional step

Please cite this article in press as: Ciri, U., et al. Dependence of leukocyte capture on instantaneous pulsatile flow. J. Biomech. (2018), https://doi.org/10.1016/j.jbiomech.2018.05.044

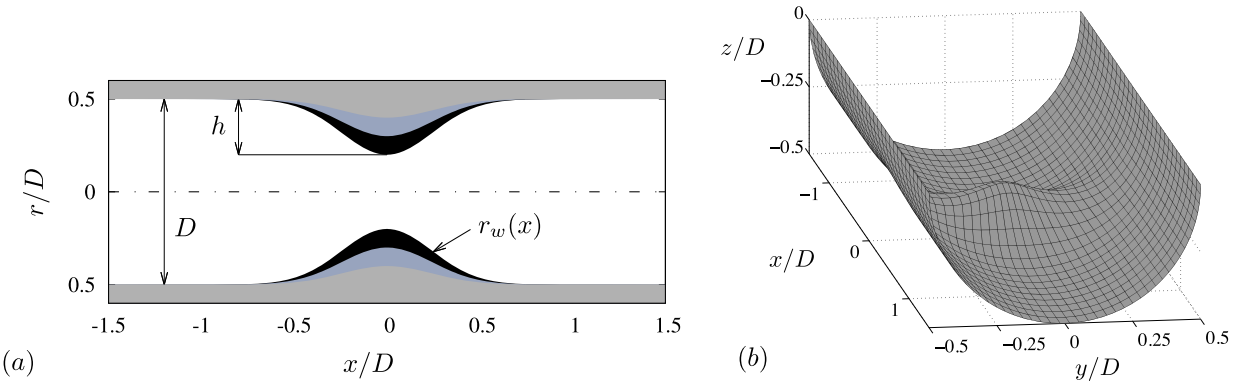


Fig. 1. Geometry of the stenoses used in the simulations: (a) cross-section along the artery axis for the axisymmetric geometry. The color shades denote the different stenosis heights h: $h = 0.1D$, $h = 0.2D$, $h = 0.3D$. (b) Visualization of the three-dimensional stenosis in the case $h = 0.2D$. Only half of the circular wall is shown. The other half is smooth. (For interpretation of the references to colour in this figure legend, the reader is referred to the web version of this article.)

method is used to update the pressure. The code is parallelized with MPI (Message Passing Interface) and simulations have been performed with 64 processors.

The computational grid is uniform, with 640 points in the streamwise direction and 128×128 points in the cross-section. At all solid walls the velocity field vanishes according to the impermeability and no-slip condition, $\mathbf{u} = 0$. The arterial wall and stenosis are reproduced using the immersed boundary method, which is described in detail in Orlandi and Leonardi (2006). The center of the stenosis, corresponding to the minimum luminal area (MLA), is positioned five diameters downstream of the inlet. The total length of the artery is $32D$. Radiative outflow conditions are prescribed at the outlet of the computational domain (Orlanski, 1976).

A model to evaluate the leukocyte capture as a function of the wall shear stress (*WSS*) was incorporated into the DNS code. The capture of leukocyte to a fully activated endothelium is affected by the local value of the shear stress. Bhui and Hayenga (2017) proposed a correlation model for the rate of capture of neutrophils as a function of the *WSS*:

$$R = \begin{cases} \frac{\rho_n}{300}\left(0.26WSS^2 - 0.8WSS + 0.63\right) & WSS \le 1.2\ \text{Pa} \\ 0 & WSS > 1.2\ \text{Pa} \end{cases} \tag{8}$$

where ρ_n is the density of the neutrophils in the blood. R represents the number of leukocytes that adhere per unit surface area per unit time (measured in units of cells per $\text{mm}^2 \cdot \text{s}$). The model was derived from published results in Sheikh et al. (2003). Analogously, according to Bhui and Hayenga (2017), an algorithm for the rate of capture for monocytes is

$$R = \begin{cases} \frac{\rho_m}{600}\left(-0.33WSS^3 + 1.4WSS^2 - 1.8WSS + 0.79\right) & WSS \le 1.0\ \text{Pa} \\ 0 & WSS > 1.0\ \text{Pa} \end{cases} \tag{9}$$

while for lymphocytes (Bhui and Hayenga, 2017):

$$R = \begin{cases} \frac{\rho_l}{25}\left(-9.93WSS^3 + 11WSS^2 - 4.1WSS + 0.55\right) & WSS \le 0.41\ \text{Pa} \\ 0 & WSS > 0.41\ \text{Pa} \end{cases} \tag{10}$$

The rules for monocyte-like cells (U937) were derived from Gonzales and Wick (1996), and for lymphocytes from Melder et al. (1995). Supplemental Fig. 1 illustrates the experimental data and capture as a function of *WSS* rule for each leukocyte. These correlations make it possible to evaluate in real-time the growth of the stenosis, as a function of the dynamical hemodynamic conditions. In order to focus on the effects of blood flow on leukocyte capture, articles that fully activate the endothelium were used. That is, in the experiments high concentrations of the cytokine Tissue Necrosis Factor-alpha (TNF-α) caused about the maximum amount of adhesion molecules and selectins to be expressed on the endothelium (Ting et al., 2007). Specifically, Sheikh et al. (2003), Gonzales and Wick (1996) and Melder et al. (1995) used 100 U/ml, 1000 U/ml and 166 ng/ml of TNF-α, respectively. Therefore, leukocyte adhesion should only depend on *WSS*, not based on receptor availability. In Eqs. (8)–(10), the absolute value of the *WSS*, measured in Pa, shall be considered. For each particular leukocyte, the concentration is measured in units of cells per mm^3 of blood. Table 1 reports the values of the leukocyte concentration considered herein, as well as other significant parameters for the simulations.

Previously, the code was extensively validated in cases of flow over rough surfaces (Orlandi et al., 2006; Burattini et al., 2008). Herein, to validate the code for pulsatile flows the same simulations were performed using a commercial software, COMSOL. Simulations with COMSOL are two-dimensional axisymmetric due to the higher computational cost. This does not significantly affect the results because the axisymmetric geometry of the stenotic wall (with $h = 0.2D$) was considered for the validation case. On the other hand, the use of our in-house code allows us to calculate the *WSS* and leukocyte capture instantaneously.

For the axisymmetric geometries, the results from the fully three-dimensional Direct Numerical Simulation (DNS) are averaged along the azimuthal direction ϑ to be consistent with COMSOL and to give the overall effect of the stenosis. Therefore, in the following sections, for the axisymmetric cases, $u = u(x, r, t)$ indicates such azimuthally-averaged velocity, and is simply referred to as the "instantaneous" velocity. The mean velocity is

Table 1
Table of parameters.

Parameter	Value
Length of artery (L)	92.8 mm
Diameter of artery (D)	2.9 mm
Blood density (ρ)	1060 kg/m^3
Blood kinematic viscosity (ν)	3.3×10^{-6} m^2/s
Mean velocity (u_{mean})	0.384 m/s
Time period of blood flow (T)	0.8 s
Womersley number (α)	2.3
Reynolds number (Re)	340
Leukocyte concentration in blood	7×10^9/l
Neutrophil concentration in blood (ρ_n)	62% of leukocytes
Monocyte concentration in blood (ρ_m)	5.3% of leukocytes
Lymphocyte concentration in blood (ρ_l)	30% of leukocytes

Please cite this article in press as: Ciri, U., et al. Dependence of leukocyte capture on instantaneous pulsatile flow. J. Biomech. (2018), https://doi.org/10.1016/j.jbiomech.2018.05.044

obtained from the time-average of u over the cardiac cycle and is denoted as $\overline{u}(x,r)$. An analogous notation is applied to the other variables. The dependence on the azimuthal position is explicitly considered for the three-dimensional geometries (as specified in Section 3.3).

The first two periods have not been included in the analysis to discard the transient of the simulation initialization. The DNS fields from the successive periods have been considered and sampled every $T/360$. A convergence check for the statistics has been performed. Using two or more periods, for the Reynolds number in the present simulation, does not change significantly the time-averaged field, nor the "instantaneous" (in the sense specified above) field phase-averaged over more cycles. However, this conclusion is not general and may not hold for different configurations. For example, previous studies have documented the onset of flow instabilities and turbulence at larger Reynolds and Womersley numbers (Mittal et al., 2001; Mallinger and Drikakis, 2002; Mittal et al., 2003; Sherwin and Blackburn, 2005; Beratlis et al., 2005, 2007; Varghese et al., 2007a,b).

3. Results and discussion

3.1. Flow field

Fig. 2 shows visualizations of the flow field during different phases of the cardiac cycle, as well as the time-averaged flow field. Streamlines are superimposed to the velocity contours to understand the flow patterns and emphasize the importance of the dynamics. The stenosis is axisymmetric and the maximum height is $h = 0.2D$. The dimensions in the figure are stretched for the sake of clarity.

The flow field averaged azimuthally and over the complete cardiac cycle is shown in Fig. 2b. In this case, the presence of the stenosis causes a convergence of the streamlines upstream the obstacle and a consequent increase in velocity. After reaching the minimum luminal area (MLA) at $x = 0$, the flow proceeds to expand downstream. The flow is not able to contour the stenotic wall because of the strong adverse pressure gradient caused by the stenosis, resulting in flow separation. The recirculating region extends for about 4 lumen diameters downstream the MLA before the flow reattaches and gradually recovers to the upstream conditions.

Normalized with the obstacle height h, the reattachment length at the mean flow rate is around $20h$ measured from the MLA. This is consistent with findings for analogous flow configurations, such as the backward-facing step. For low Reynolds number, the reattachment length can reach up to 10–15 step heights (Macagno and Hung, 1967; Goldstein et al., 1970; Denham and Patrick, 1974; Armaly et al., 1983; Fabiani et al., 2009), while it is much shorter ($\simeq$ 5–6h) as the Reynolds number increases and the flow transitions to turbulence (Le et al., 1997; Leonardi et al., 2003).

Each phase of the cardiac cycle presents a quite different flow field, due to the high variability of the pulsatile mass-flow rate. Fig. 2c–f show the velocity and the streamlines at four instants during the cardiac cycle (Fig. 2a). At the minimum flow rate ($t/T = 6/32$, Fig. 2c), two recirculating regions form upstream and downstream the stenosis and extend over the whole domain. Close to the wall, the flow is reversed, while a slow forward stream still persists in the central region of the lumen.

When the aortic valve closes ($t/T = 14/32$, Fig. 2d), and diastole commences, the flow rate begins to increase again as anterograde motion is restored across the coronary artery. A single recirculating region downstream the MLA is formed, but is considerably shorter than for the time-averaged field. The flow reattaches quickly because of the relatively low acceleration through the stenosis. The separated region reaches its largest length and intensity at the maximum instantaneous flow rate ($t/T \approx 18/32$, Fig. 2e). The streamlines in the recirculating region are closer to each other, which means the reverse flow is stronger compared to the mean field (Fig. 2b) or the other phases. Towards the end of diastole, the instantaneous field resembles the mean field as the instantaneous bulk velocity is close to the time-averaged value (e.g. at $t/T = 30/32$, Fig. 2f).

Fig. 3 compares the results of the present simulation with velocity profiles obtained using the commercial software COMSOL. The profiles are sampled at four equally spaced instants of the cardiac cycle 1.615 mm upstream the MLA (Fig. 3a–b), at the MLA (Fig. 3e–h), and 1.615 mm downstream the MLA (Fig. 3i–l).

A quantitative measure of the difference between the two CFD solvers is provided by the normalized mean square error ($NMSE$):

$$NMSE(x,t) = \frac{\langle (u_{\mathrm{COMSOL}} - u_{\mathrm{DNS}})^2 \rangle_r}{\langle u_{\mathrm{COMSOL}} \rangle_r \cdot \langle u_{\mathrm{DNS}} \rangle_r}, \tag{11}$$

where $\langle \cdot \rangle_r$ indicates an average along the radial direction. The maximum NMSE between the two simulations is about 3% downstream

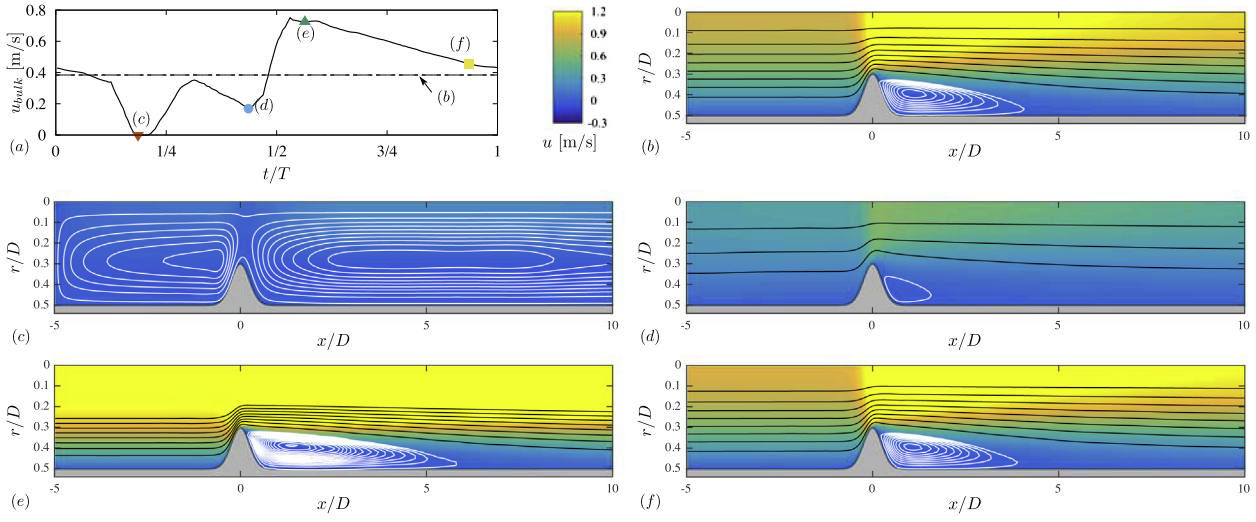


Fig. 2. Flow field during a cardiac cycle: (a) cardiac cycle: ——— instantaneous bulk velocity; – – – – mean bulk velocity. (b) Mean flow field averaged over a cardiac cycle. (c)–(f) Instantaneous flow fields: (c) $t/T = 6/32$ ▼, (d) $t/T = 14/32$ ●, (e) $t/T = 18/32$ ▲, (f) $t/T = 30/32$ ■. The scales of the axes in the figures are different to show the details of the flow past the stenosis.

Please cite this article in press as: Ciri, U., et al. Dependence of leukocyte capture on instantaneous pulsatile flow. J. Biomech. (2018), https://doi.org/10.1016/j.jbiomech.2018.05.044

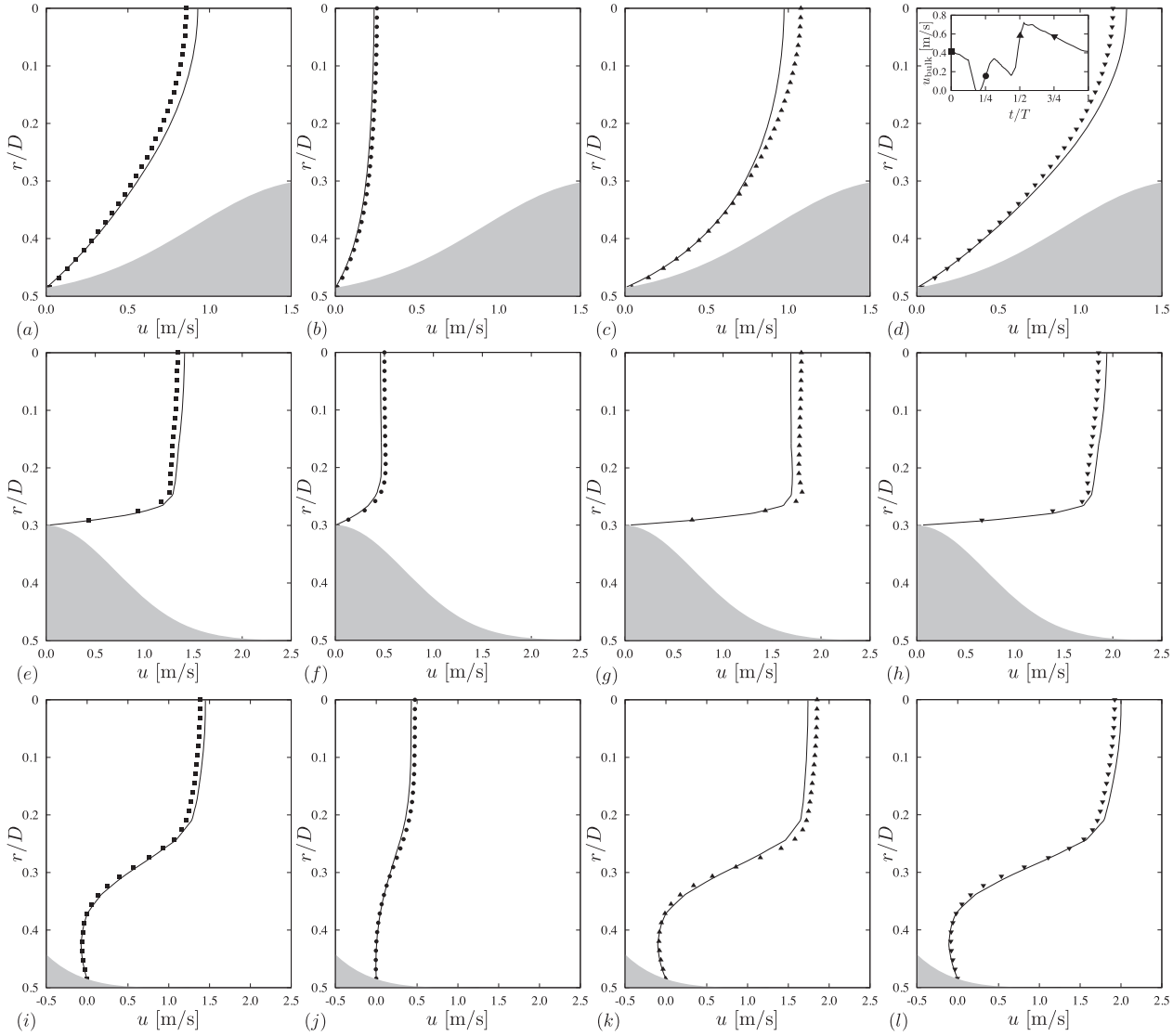


Fig. 3. Velocity profiles at 1.615 mm ($x/D \approx 0.55$) upstream the MLA (a–d), at the MLA (e–h), and 1.615 mm downstream the MLA (i–l) at different instants during the cardiac cycle: ■ $t/T = 0$; • $t/T = 1/4$; ▲ $t/T = 1/2$; ▼ $t/T = 3/4$. Line represents the COMSOL simulation; symbols represent our in-house code results. The shaded region represents the shape and position of the plaque in the coronary.

the MLA at $t = T/4$; otherwise the error is lower than 2%. Note that the error is relative to the instantaneous mean velocity in the lumen. At $t = T/4$ the incoming flow rate is near the minimum (Fig. 2a) and the instantaneous mean velocity is quite low. In absolute terms, the maximum *NMSE* corresponds to a difference of 0.07 m/s between COMSOL and our in-house code. The absolute maximum difference (that is max $|u_{COMSOL} - u_{DNS}|$) is about 0.2 m/s downstream the MLA at $t = T/2$ (Fig. 3k).

In general, the larger discrepancies are observed downstream the MLA. Indeed, this region of the domain is the most challenging to predict, because of the presence of separated flow (Fig. 2). Nonetheless, the profile in the near-wall region is quite similar for both simulations. The differences in the outer layer at $x = 1.615$ mm are probably inherited from the differences in the profile upstream the stenosis (Fig. 3a–d), rather than due to the flow evolution through the obstacle.

The DNS suggests the presence of a local jet close to the wall at the MLA at high flow rate (Fig. 3g, h), which is not evident in the COMSOL simulation. The stenotic wall induces the flow to converge towards the centre (see the streamlines in Fig. 2e), which causes a local acceleration. Nevertheless, its magnitude is quite small and the shapes of the profiles are still quite similar.

3.2. Wall shear stress and rate of capture

Hemodynamic conditions influence the rate of leukocyte adhesion, extravasation, compositional changes and ultimately growth of a stenotic plaque (Gibson et al., 1993; Chatzizisis et al., 2008; Timmins et al., 2015; Samady et al., 2011; Burns et al., 2007; Sheikh et al., 2003; Barreiro et al., 2005; Cinamon and Alon, 2003). Specifically, the local value of *WSS* significantly influences whether a leukocyte will be captured and then adhere to the endothelium or not. Bhui and Hayenga (2017) proposed a correlation model for the rate of capture of different leukocytes as a function of the wall shear stress (*WSS*), see Eqs. (8)–(10). The algorithm has been implemented in our in-house code to compute on-line the rate of capture *R* based on the instantaneous flow conditions (i.e. *WSS*).

The local wall shear stress *WSS* can be computed as:

Please cite this article in press as: Ciri, U., et al. Dependence of leukocyte capture on instantaneous pulsatile flow. J. Biomech. (2018), https://doi.org/10.1016/j.jbiomech.2018.05.044

$$WSS = \mu \left. \frac{\partial U}{\partial n} \right|_{r=r_w(x)} \tag{12}$$

where U is the velocity tangential to wall (which depends on the streamwise and radial components), n is the normal to the wall, and $\mu = \rho\nu$ is the blood dynamic viscosity. Fig. 4a shows the value of *WSS* along the artery wall averaged in the azimuthal direction and in time over the cardiac cycle.

At the inlet of the domain ($x < 0$), the value of *WSS* coincides with the theoretical value for a straight circular pipe:

$$WSS_0 = \frac{8}{Re}\,\rho u_{\text{mean}}^2 \approx 4 \text{ Pa} \tag{13}$$

This time-averaged *WSS* in the healthy region of the artery is larger than the maximum *WSS* (1.2 Pa) that a neutrophil is able to withstand and remain adhered to the endothelium, see Eq. (8). In fact, the lumen is unobstructed far upstream of the stenosis and therefore the flow is not affected by the stenosis. As the flow approaches the stenosis, the wall shear rapidly increases and reaches a peak at the MLA. As the flow separates due to the strong adverse pressure gradient, *WSS* drops and becomes negative in the recirculating region (Fig. 2). Further downstream, the flow recovers the unperturbed conditions and the shear returns to the expected value for a straight pipe, WSS_0. This confirms that the length of our computational domain is adequate. The evolution of the wall shear stress is in qualitative agreement with the numerical simulations of Mittal et al. (2001) and Varghese et al. (2007a,b) for similar stenotic geometries.

However, time-averaged *WSS* ignores significant incremental features over instantaneous flow throughout the cardiac cycle and may underpredict plaque growth. Fig. 4b shows the *WSS* at four different phases of the cardiac cycle (see Fig. 2a), as well as

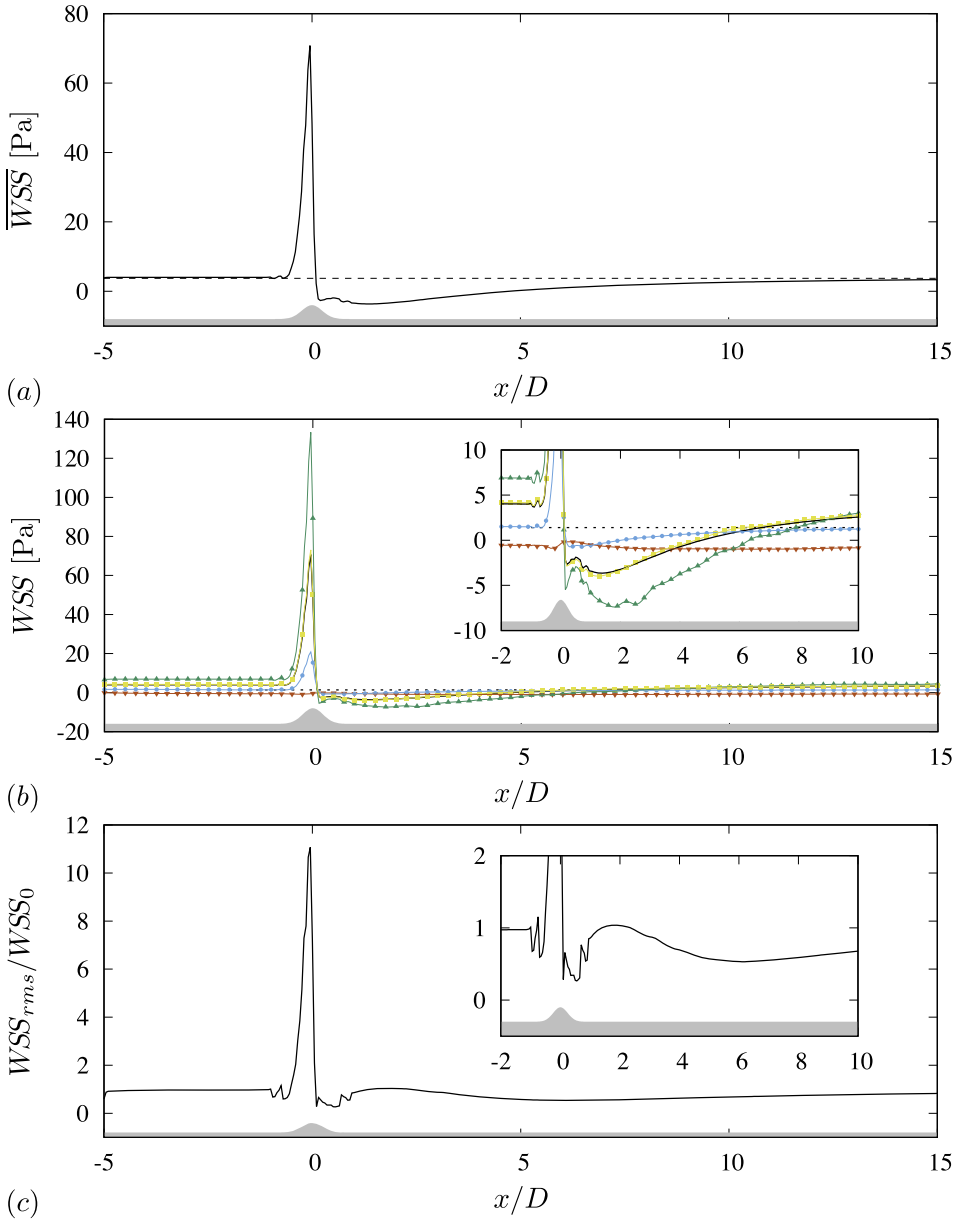


Fig. 4. Wall shear stress along the artery: (a) $\overline{WSS}$, as a function of the streamwise coordinate: ——— DNS, – – – – theoretical value for a circular pipe, according to Eq. (13); (b) instantaneous wall shear stress: ▼ $t/T = 6/32$, ● $t/T = 14/32$, ▲ $t/T = 18/32$, ■ $t/T = 30/32$; ——— time-averaged $\overline{WSS}$; ····· value of *WSS* above which leukocytes cannot adhere, $WSS = 1.2$ Pa. (c) Root mean square value of *WSS* normalized by the healthy value WSS_0.

Please cite this article in press as: Ciri, U., et al. Dependence of leukocyte capture on instantaneous pulsatile flow. J. Biomech. (2018), https://doi.org/10.1016/j.jbiomech.2018.05.044

the value averaged over the whole cycle ($\overline{WSS}$). At the minimum inflow rate ($t/T = 6/32$), the *WSS* is negative at all streamwise locations because of the reverse flow. In addition, even if we consider the absolute values, the *WSS* is always less than the threshold of 1.2 Pa, and therefore susceptible to leukocyte capture. On the other hand, at the maximum flow rate ($t/T = 18/32$) the WSS reaches its peak value at MLA of about 130 Pa, which is almost double the maximum value of the mean distribution. In contrast, the instantaneous *WSS* is close to the mean distribution ($\overline{WSS}$) at $t/T = 30/32$, when the incoming flow rate is about the same as the mean flow rate. Fig. 2f also shows that in this case the flow field is quite similar to the mean flow field (Fig. 2b).

The region of negative *WSS* (shown in the inset of Fig. 4b) depends on the topology of the recirculation bubble. The largest extent is at the maximum flow rate ($t/T = 18/32$). Nonetheless, in this case the stress at the wall is larger, in absolute value, than the capture threshold, because of the high intensity of the reverse flow. On the other hand, at $t/T = 14/32$, the separated region is much shorter and the *WSS* is below 1.2 Pa, so the leukocytes have the ability to adhere to the endothelial wall.

Fig. 4c shows the root mean square (rms) value of wall shear stress, WSS_{rms}, normalized with the healthy value WSS_0. WSS_{rms} is computed with respect to the azimuthally- and time-averaged local shear stress. The wall shear stress varies quite strongly near the MLA, where the flow experiences the largest gradients. Nonetheless, the rms value is almost as large as WSS_0 along most of the artery, owning the variability of the pulsatile inflow (Fig. 2a). Since the neutrophil capture (8) is non-linearly dependent on shear stress, the variations during the cycle represented by WSS_{rms} will certainly influence the rate of leukocyte capture.

The rate of neutrophil capture has been computed with the model (8) using the instantaneous *WSS* predicted by our in-house code. Fig. 5a shows the rate of capture per unit area and time at four instants during the cardiac cycle (see Fig. 2a).

The mean rate of capture, averaged over the complete period, $\overline{R(WSS)}$ is also superimposed to the instantaneous distributions along the artery. This has been computed from the instantaneous wall shear stress obtained from the DNS as:

$$\overline{R(WSS)} = \frac{1}{T}\int_0^T R(WSS(t))\,\mathrm{d}t \tag{14}$$

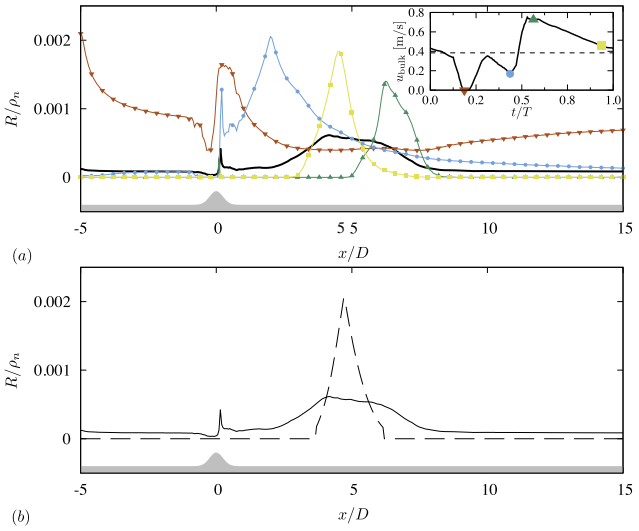


Fig. 5. Neutrophil capture *R* due to the *WSS*. (a) Capture rate throughout the cardiac cycle: ▼ $t/T = 6/32$, ● $t/T = 14/32$, ▲ $t/T = 18/32$, ■ $t/T = 30/32$; ——— time-averaged $\overline{R(WSS)}$. (b) Comparison between using rate of capture from the mean shear, $R(\overline{WSS})$, (– – – –) and the actual mean rate of capture, $\overline{R(WSS)}$, (———).

At the minimum flow rate ($t/T = 6/32$), chance of adhesion takes place along the whole artery wall, given the low level of *WSS*. The other time instants are generally characterized by two peaks in the capture rate, which correspond to the separation and reattachment points, for which $WSS = 0$. As the flow separation is rather abrupt (see the drastic change in *WSS* in Fig. 4b), the upstream peak is sharp and encloses a small area downstream the MLA. The reattachment process is more gradual and the downstream capture peak is spread over a larger distance. Far from the stenosis the capture rate is generally small, as the disturbance due to the plaque is small. In these segments, the mean rate of capture is on the same level of that of a straight artery (without stenosis, see Appendix A).

At $t/T = 14/32$ the incoming mass flow rate is relatively low and the leukocyte capture is enabled in the region of recirculating flow (Fig. 2d). On the contrary at $t/T = 18/32$ (maximum flow rate), the reverse flow is strong (Fig. 2e) and the consequent *WSS* is too large (although negative, Fig. 4b) to permit capture in the central region of the recirculation bubble. In this case, capture is observed only nearby the reattachment and separation points.

Even though the instantaneous distribution of *WSS* at $t/T = 30/32$ is similar to the mean distribution (Fig. 4b), the instantaneous rate of capture is significantly different from the mean rate of capture. This is expected as a result of the non-linear correlation between neutrophil capture and the *WSS*, Eq. (8). In general, the qualitative differences observed between the instantaneous distributions of the neutrophil capture rates, *R*, and the mean capture curve are more pronounced than the analogous discrepancies observed for other quantities (for example, the *WSS*, Fig. 4b).

The instantaneous flow over a cardiac cycle influences leukocyte capture. For convenience, usually only the mean *WSS* is calculated a posteriori to determine the rate of capture, that is

$$\overline{WSS} = \frac{1}{T}\int_0^T WSS(t)\,\mathrm{d}t \tag{15}$$

is used in Eq. (8). Fig. 5b shows that this rate of capture computed from the mean stress ($R(\overline{WSS})$) is considerably different from the actual mean rate of capture $\overline{R(WSS)}$, Eq. (14). The rate of capture in Eq. (14) is obtained with the instantaneous value of the *WSS*. The capture rate from the mean shear $R(\overline{WSS})$ is rather similar to the instantaneous capture rate at $t/T = 30/32$ and, for instance, does not include at all the effect of the low mass-rate interval of the cardiac cycle, which causes capture along the whole luminal wall of the artery. The capture downstream the stenosis (around $x/D \approx 5$) is also over-predicted because the mean shear distribution $\overline{WSS}$ fails to consider the fluctuations of the reattachment point, which moves upstream and downstream over the cardiac cycle (Fig. 2). Results in Fig. 5b imply that the growth of the plaque predicted using the average *WSS* may be significantly different than that considering the real dynamics of the flow.

Fig. 6 shows the mean rate of capture $\overline{R(WSS)}$ (calculated with the instantaneous value of the *WSS*) for three different types of leukocytes: neutrophils, monocytes and lymphocytes.

The rate of capture for monocytes has been computed using the algorithm based on Eq. (9), while for lymphocytes Eq. (10) has been used. Note that the results in Fig. 6a are per unit concentration of the leukocytes in the blood. In practice, the actual capture of a leukocyte type will also depend on the concentration of the particular leukocyte in the blood. For instance, the concentration of monocytes is the lowest (Table 1), and the actual capture rate is practically negligible compared to lymphocytes and neutrophils (Fig. 6b). On the other hand, neutrophil capture is equivalent to lymphocytes simply due to the fact that the concentration of neutrophils in the blood is higher than that of lymphocytes, yet the

Please cite this article in press as: Ciri, U., et al. Dependence of leukocyte capture on instantaneous pulsatile flow. J. Biomech. (2018), https://doi.org/10.1016/j.jbiomech.2018.05.044

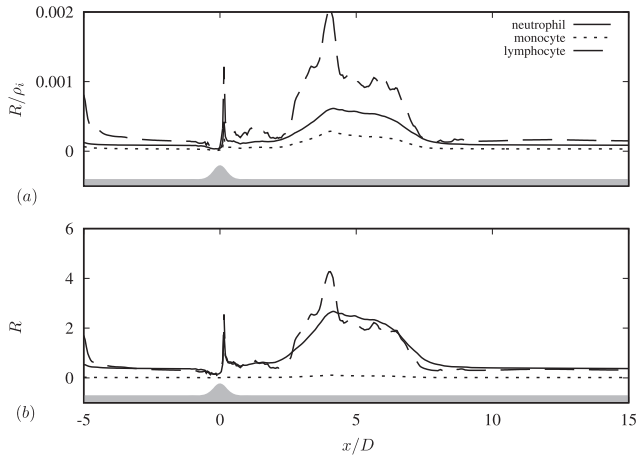


Fig. 6. Mean rate of capture $\overline{R(WSS)}$ for different types of leukocytes: ———neutrophil, ·····monocyte, – – – –lymphocyte. (a) Per unit concentration ρ_i (where i indicates the type of leukocytes); (b) actual capture rate.

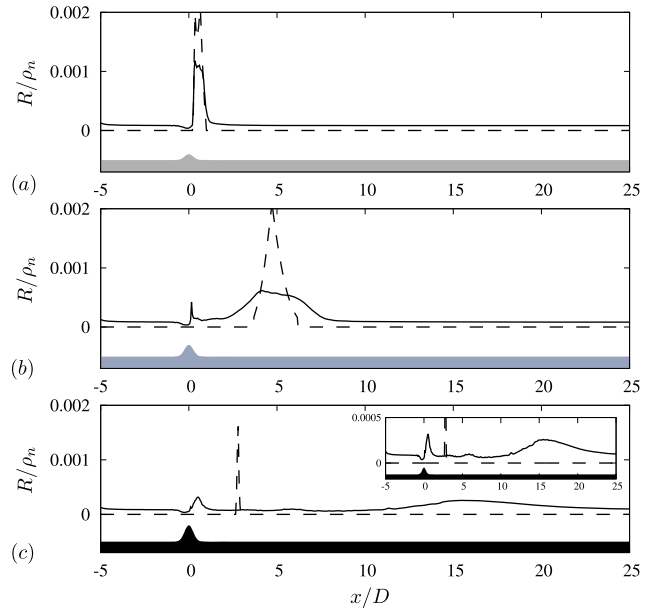


Fig. 7. Neutrophil capture rate for different stenosis heights: ———mean rate from instantaneous shear stress $\overline{R(WSS)}$; – – – – capture rate using time-averaged wall shear stress $R(\overline{WSS})$. (a) $h = 0.1D$; (b) $h = 0.2D$ (same as Fig. 5b); (c) $h = 0.3D$, the scale in the inset is changed to emphasize the details of the mean capture rate distributions, $\overline{R(WSS)}$.

overall rate of capture per unit concentration is lower than for lymphocytes.

From a qualitative point of view, the distribution of leukocyte capture is quite similar for all three types of leukocytes (Fig. 6a). The main region of capture is downstream the stenosis ($3 \lesssim x/D \lesssim 7$) and is related to the flow reattachment. Although the site of capture and adhesion roughly corresponds to the site of transmigration and plaque development, there are some factors that influence this process. For example, after a leukocyte adheres to the endothelium, it may take anywhere from seconds to several minutes to extravasate through the endothelium (Hayenga and Aranda-Espinoza, 2013; Stroka et al., 2013). During this time, leukocytes typically migrate a few micrometers from their original adhesion spot on the endothelium before extravasating. Once inside the arterial wall, leukocyte migration is directed according to chemotaxis, durotaxis, and physical constraints. Thus, regions with a high R value do not directly indicate areas of plaque growth. That being said, qualitatively regions with high leukocytes adhesion will have a lot of cytokine production from the incoming cells. Therefore, a secondary plaque may start to form, apart from the main lesion location. Overall these studies inform why often times angiography reveals patients with atherosclerosis do not only have one lesion, but multiple (Goldstein et al., 2000).

As the plaque grows, the hemodynamic patterns will change accordingly and further affect the growth. An agent-based model for extravasation and adhesion, analogous to the rules (8)–(10) for capture, is required to model the full process in order to account for actual modifications of the artery wall. If such model is available, the change in the shape of the stenosis can be handled with the immersed boundary method with almost negligible additional computational costs. Incorporation of a leukocyte adhesion with transmigration model would allow for direct simulation of plaque growth. Herein we present capture patterns as a result of instantaneous and time-averaged blood flow.

3.3. Effect of the stenosis geometry

To characterize more in depth the effect of the wall geometry, we have performed a parametric study varying the height of the stenosis. For the axisymmetric model, we have considered three different values for the peak height of the stenosis, specifically $h/D = 0.1, 0.2, 0.3$. Fig. 7 shows the neutrophil capture rate for the three different cases. For each stenosis geometry, the capture is computed both averaging the capture rate due to the instantaneous wall shear, $\overline{R(WSS)}$, and using only the time-averaged wall shear, $R(\overline{WSS})$.

For the smallest stenosis height ($h = 0.1D$, Fig. 7a), there is not a large difference between the two distributions. The obstruction to the blood stream is small, hence the flow patterns downstream the MLA do not show a large variability. In this case, the mean flow provides a close approximation for the mean rate of capture during a cardiac cycle. As the size of the obstacle grows, the topology of the recirculation bubble varies significantly during the cardiac cycle, as shown in the visualization in Fig. 2. Consequently, the differences between the two distributions become sizeable.

As the value of h increases, the downstream capture region, related to the flow reattachment point, moves further downstream. In the low Reynolds number regime, the length of the recirculation bubble is roughly proportional to the local Reynolds (based on the obstacle height). Thus the flow reattaches at larger distance from the MLA with increasing h. For $h = 0.3D$, the flow starts to exhibit instabilities downstream the MLA, especially during high flow-rate period of the cardiac cycle ($t \gtrsim T/2$). This is because locally the Reynolds number at the MLA can be quite large due to the flow acceleration, which increases with stronger obstructions (that is larger h). In the turbulent regime, the recirculation region is shorter (Leonardi et al., 2003). The time-averaged shear stress distribution is affected by this change of regime, and the neutrophil capture peak computed from $R(\overline{WSS})$ is observed closer to the MLA.

The capture rate for the cases with three-dimensional stenosis is reported in Fig. 8. The rate of capture for neutrophils is represented with color contours super-imposed over the artery wall. For the three-dimensional case, no average along the azimuthal direction is performed, since the heterogeneity of the geometry reflects in non-uniform flow properties along the azimuthal direction. Thus, the wall shear stress is computed from the local velocity gradient, normal to the wall surface. In Fig. 8, only the region close to the MLA (up to $1.5D$ downstream) is shown because the capture is not observed at larger distance from the peak of the stenosis. The differences between the mean rate of capture $\overline{R(WSS)}$ and the

Please cite this article in press as: Ciri, U., et al. Dependence of leukocyte capture on instantaneous pulsatile flow. J. Biomech. (2018), https://doi.org/10.1016/j.jbiomech.2018.05.044

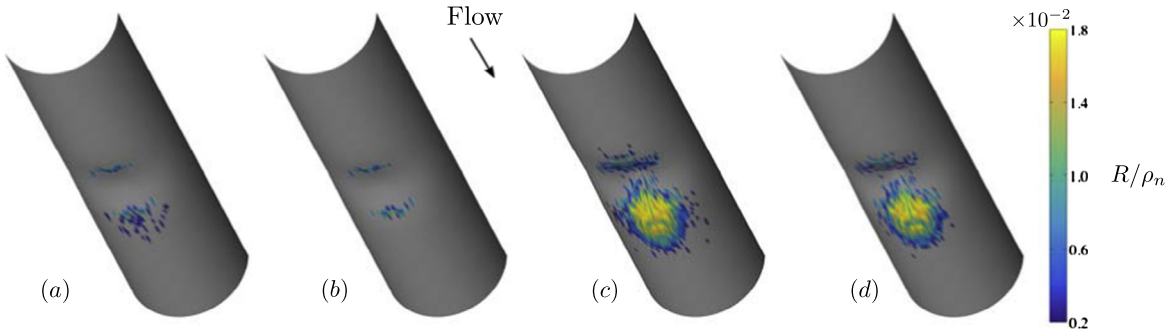


Fig. 8. Neutrophil rate of capture for the three dimensional stenosis: (a, b) $h = 0.1D$; (c, d) $h = 0.2D$. In (a) and (c), the capture rate is computed averaging the instantaneous capture over the cardiac cycle, $\overline{R(WSS)}$; in (b) and (d), capture is computed using the time-averaged shear stress, $R(\overline{WSS})$.

capture computed from the mean shear $R(\overline{WSS})$ are limited. The area occluded by the stenosis is about 6% and 12% of the healthy lumen for $h = 0.1D$ and $h = 0.2D$, respectively. Thus, the disturbance on the blood stream is small, and, similarly to the axisymmetric case for $h = 0.1D$, the two capture distributions are similar.

These results suggest that in the early stages of the disease the use of the time-averaged $\overline{WSS}$ to compute the capture rate may be good enough. However, as plaque grows, the flow features in each phase of the cardiac cycle become important in terms of leukocyte capture, and the use of only mean flow information may underpredict the capture rate.

4. Limitations

In this study, the stenosis geometry has been defined using regular three-dimensional or axisymmetric shapes, which affects blood flow patterns observed. For example, the axisymmetric stenosis geometries give rise to an axisymmetric flow, despite no a priori symmetry hypothesis being made. This has been done to highlight the difference between instantaneous and time-averaged flow fields, and its consequences on leukocyte capture, limiting the effect of additional factors, such as complex artery geometry. A realistic case will exhibit a more heterogeneous geometry and, consequently, flow patterns. In this case, significant differences in the *WSS* could be present along the coronary circumference at the same time instants due to the complex artery geometry (Ku et al., 1985). Therefore, also the spatial, as well as temporal, distribution of *WSS* may affect the local capture rate and atherogenesis. Nevertheless, the computations carried out with our in-house code are fully three-dimensional and do not rely on a priori symmetry hypotheses. The present methodology can be employed also for irregular realistic stenotic configurations. Moreover, direct numerical simulations are able to resolve turbulent flow, which may eventually be induced in the stenotic artery for suitable values of the Reynolds and Womersley number (Mittal et al., 2001; Mallinger and Drikakis, 2002; Mittal et al., 2003; Sherwin and Blackburn, 2005; Beratlis et al., 2005, 2007).

In this study leukocyte capture was based solely on *WSS*, with a fully activated endothelium (with TNF-α). The degree of activation is defined as the expression level of leukocyte binding selectins and adhesion molecules on the endothelium. Physiologically, the endothelium may be only partially activated (as in the case of low concentrations of TNF-α) resulting in spatially heterogeneous levels of activation. Intuitively, when the degree of endothelial activation is low the effects of *WSS* would be less significant. Therefore, a potential limitation with this study is that the endothelium is considered fully activated. Thus, in the case of low activation the effects of time-dependent *WSS* versus time-averaged *WSS* on leukocyte adhesion may not be as noticeable.

5. Final remarks

In this study we used in-house DNS to investigate the flow patterns around a stenotic coronary artery. In the model, physiological conditions were imposed by using the immersed boundary method to model the stenosis, unsteady three-dimensional Navier-Stokes equations to model the flow, and a pulsating triphasic waveform at the inlet to mimic the cardiac cycle. The present results agree well with those obtained from a commercial software, COMSOL.

We emphasize the importance of taking into account the unsteadiness of the flow over the cardiac cycle in determining leukocyte capture rate. The instantaneous flow field can be quite different from the mean flow given the large variability of the incoming mass flow rate. In particular, predicting the rate of capture of leukocytes can be inaccurate if solely based on the mean flow field and wall shear stress (*WSS*). Owing to the complexity of the leukocyte transmigration process, the capture conditions can significantly vary over the entire cardiac cycle. In general, the mean *WSS* underestimates the total amount of leukocyte captured over the span of the cardiac cycle. Therefore, it is recommended that CFD simulation be coupled with a leukocyte transmigration model, so that the instantaneous *WSS* distribution is considered to evaluate the leukocyte rate of capture. This way a more accurate estimate of the stenosis growth can be obtained. Unfortunately, this may not be straightforward when using a commercial software because it requires the implementation of the capture model in the CFD code. Otherwise, one could take an alternative approach as was done, for example, in Bhui and Hayenga (2017) by discretizing the cardiac cycle and evaluating the capture rate for a number of sub-intervals.

Conflict of interest

The authors declare no conflict of interest.

Acknowledgements

Authors gratefully acknowledge funding for this work provided by the American Heart Association (17SDG33400239) and by the National Heart, Lung, And Blood Institute of the National Institutes of Health under Award Number R01HL136776. The content is solely the responsibility of the authors and does not necessarily represent the official views of the National Institutes of Health.

Appendix A. Straight artery

An additional simulation has been carried out for reference of an artery without stenosis, using the same setup described in Section 2. Fig. 9 shows the mean rate of capture for neutrophils for the

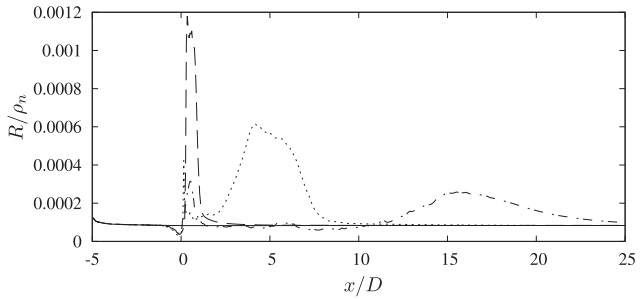


Fig. 9. Mean rate of neutrophil capture, $\overline{R(WSS)}$, for different artery geometry: ———straight pipe (no stenosis); – – – –$h/D = 0.1$; ·····$h/D = 0.2$; —·—·— $h/D = 0.3$.

various (axisymmetric) geometries considered herein, including the straight artery.

Neutrophil capture is negligible along the wall of a straight artery. The presence of the stenosis induces a peak in the capture rate, which moves downstream as the degree of flow obstruction increases. However, relatively far from the MLA (in terms of maximum stenosis height h), the capture rate attains the same minimal level as the straight artery. This confirms that the domain of the DNS has an adequate length, which permits to capture the effects of the stenosis and to recover unperturbed flow conditions.

Appendix B. Supplementary material

Supplementary data associated with this article can be found, in the online version, at https://doi.org/10.1016/j.jbiomech.2018.05.044.

References

Armaly, B.F., Durst, F., Pereira, J.C.F., Schönung, B., 1983. Experimental and theoretical investigation of backward-facing step flow. J. Fluid Mech. 127, 473–496.

Bailey, A.M., Thorne, B.C., Peirce, S.M., 2007. Multi-cell agent-based simulation of the microvasculature to study the dynamics of circulating inflammatory cell trafficking. Ann. Biomed. Eng. 35 (6), 916–936. https://doi.org/10.1007/s10439-007-9266-1. PubMed PMID: 17436112.

Barreiro, O., Yanez-Mo, M., Sala-Valdes, M., Gutierrez-Lopez, M.D., Ovalle, S., Higginbottom, A., Monk, P.N., Cabanas, C., Sanchez-Madrid, F., 2005. Endothelial tetraspanin microdomains regulate leukocyte firm adhesion during extravasation. Blood 105 (7), 2852–2861. https://doi.org/10.1182/blood-2004-09-3606. PubMed PMID: 15591117.

Beratlis, N., Balaras, E., Parvinian, B., Kiger, K., 2005. A numerical and experimental investigation of transitional pulsatile flow in a stenosed channel. J. Biomech. Eng. 127, 1147–1157.

Beratlis, N., Balaras, E., Kiger, K., 2007. Direct numerical simulations of transitional pulsatile flow through a constriction. J. Fluid Mech. 587, 425–451.

Bhui, R., Hayenga, H.N., 2017. An agent-based model of leukocyte transendothelial migration during atherogenesis. PLoS Comput. Biol. 13 (5), e1005523. https://doi.org/10.1371/journal.pcbi.1005523.

Burattini, P., Leonardi, S., Orlandi, P., Antonia, R.A., 2008. Comparison between experiments and direct numerical simulations in a channel flow with roughness on one wall. J. Fluid Mech. 600, 403–426.

Burns, A.R., Zheng, Z., Soubra, S.H., Chen, J., Rumbaut, R.E., 2007. Transendothelial flow inhibits neutrophil transmigration through a nitric oxide-dependent mechanism: potential role for cleft shear stress. Am. J. Physiol. Heart Circ. Physiol. 293 (5), H2904–H2910. https://doi.org/10.1152/ajpheart.00871.2007. PubMed PMID: 17720767.

Chaichana, T., Sun, Z., Jewkes, J., 2012. Computational fluid dynamics analysis of the effect of plaques in the left coronary artery. Comput. Math. Methods Med. 2012, 504367. https://doi.org/10.1155/2012/504367.

Chatzizisis, Y.S., Jonas, M., Coskun, A.U., Beigel, R., Stone, B.V., Maynard, C., Gerrity, R.G., Daley, W., Rogers, C., Edelman, E.R., Feldman, C.L., Stone, P.H., 2008. Prediction of the localization of high-risk coronary atherosclerotic plaques on the basis of low endothelial shear stress: an intravascular ultrasound and histopathology natural history study. Circulation 117 (8), 993–1002. https://doi.org/10.1161/CIRCULATIONAHA.107.695254. PubMed PMID: 18250270.

Cinamon, G., Alon, R., 2003. A real time in vitro assay for studying leukocyte transendothelial migration under physiological flow conditions. J. Immunol. Methods 273, 53–62. PubMed PMID: 12535797.

Denham, M.K., Patrick, M.A., 1974. Laminar flow over a downstream-facing step in a two-dimensional channel. Trans. Inst. Chem. Eng. 52, 361–367.

Fabiani, F., Orlandi, P., Leonardi, S., 2009. Linear stability of 2D rough channels. In: Eckhardt, B. (Ed.), Advances in Turbulence XII. Springer, Berlin, Heidelberg, pp. 103–106.

Gibson, C.M., Diaz, L., Kandarpa, K., Sacks, F.M., Pasternak, R.C., Sandor, T., Feldman, C., Stone, P.H., 1993. Relation of vessel wall shear stress to atherosclerosis progression in human coronary arteries. Arterioscler. Thromb. 13 (2), 310–315.

Goldstein, J.A., Demetriou, D., Grines, C.L., Pica, M., Shoukfeh, M., O'Neill, W.W., 2000. Multiple complex coronary plaques in patients with acute myocardial infarction. N. Engl. J. Med. 343, 915–922. https://doi.org/10.1056/NEJM200009283431303.

Goldstein, R.J., Eriksen, V.L., Olson, R.M., Eckert, E.R.G., 1970. Laminar separation, reattachment, and transition of the flow over a downstream-facing step. J. Basic Eng.–T.A.S.M.E. 92, 732–739.

Gonzales, R.S., Wick, T.M., 1996. Hemodynamic modulation of monocytic cell adherence to vascular endothelium. Ann. Biomed. Eng. 24 (3), 382–393. Epub 1996/05/01. PubMed PMID: 8734059.

Hasan, M., Rubenstein, D.A., Yin, W., 2013. Effects of cyclic motion on coronary blood flow. Journal of biomechanical engineering 135 (12), 121002.

Hayenga, H.N., Aranda-Espinoza, H., 2013. Stiffness increases mononuclear cell transendothelial migration. Cel. Mol. Bioeng. 6 (3), 253–265. https://doi.org/10.1007/s12195-013-0284-9.

He, X., Ku, D.N., 1996. Pulsatile flow in the human left coronary artery bifurcation: average conditions. J. Biomech. Eng. 118 (1), 74–82.

Ku, D.N., Giddens, D.P., Zarins, C.K., Glagov, S., 1985. Pulsatile flow and atherosclerosis in the human carotid bifurcation. Arterioscl. Throm. Vas. 5, 293–302. https://doi.org/10.1161/01.ATV.5.3.293.

Le, H., Moin, P., Kim, J., 1997. Direct numerical simulation of turbulent over a backward-facing step. J. Fluid Mech. 330, 349–374.

Leonardi, S., Orlandi, P., Smalley, R.J., Djenidi, L., Antonia, R.A., 2003. Direct numerical simulations of turbulent channel flow with transverse square bars on one wall. J. Fluid Mech. 491, 229–238.

Macagno, E.O., Hung, T.K., 1967. Computational and experimental study of a captive annular eddy. J. Fluid Mech. 28, 43–64.

Mallinger, F., Drikakis, D., 2002. Instability in three-dimensional, unsteady, stenotic flows. Intl. J. Heat Fluid Fl. 23, 657–663.

Mittal, R., Simmons, S.P., Udaykumar, H.S., 2001. Application of large-eddy simulation to the study of pulsatile flow in a modeled arterial stenosis. J. Biomech. Eng. 123, 325–332.

Mittal, R., Simmons, S.P., Najjar, F., 2003. Numerical study of pulsatile flow in a constricted channel. J. Fluid Mech. 485, 337–378.

Melder, R.J., Munn, L.L., Yamada, S., Okhubo, C., Jain, R.L., 1995. Selectin- and integrin-mediated T-lymphocyte rolling and arrest on TNF-alpha-activated endothelium: augmentation by erythrocytes. Biophys J. 69 (5), 2131–2138. https://doi.org/10.1016/S0006-3495(95)80087-1. PubMed Central PMCID: PMC1236447. PubMed PMID: 8580357.

Orlandi, P., 2000. Fluid Flow Phenomena: A numerical toolkit. Kluwer Academic Publisher, Dordrecht.

Orlandi, P., Leonardi, S., 2006. DNS of turbulent channel flows with two- and three dimensional roughness. J. Turbul. 7, N53.

Orlandi, P., Leonardi, S., Antonia, R.A., 2006. Turbulent channel flow with either transverse or longitudinal roughness elements on one wall. J. Fluid Mech. 561, 279–305.

Orlanski, I., 1976. A simple boundary condition for unbounded hyperbolic flows. J. Comput. Phys. 21 (3), 251–269.

Samady, H., Eshtehardi, P., McDaniel, M.C., Suo, J., Dhawan, S.S., Maynard, C., Timmins, L.H., Quyyumi, A.A., Giddens, D.P., 2011. Coronary artery wall shear stress is associated with progression and transformation of atherosclerotic plaque and arterial remodeling in patients with coronary artery disease. Circulation 124 (7), 779–788. https://doi.org/10.1161/CIRCULATIONAHA.111.021824. PubMed PMID: 21788584.

Sheikh, S., Rainger, G.E., Gale, Z., Rahman, M., Nash, G.B., 2003. Exposure to fluid shear stress modulates the ability of endothelial cells to recruit neutrophils in response to tumor necrosis factor-alpha: a basis for local variations in vascular sensitivity to inflammation. Blood 102 (8), 2828–2834.

Sherwin, S.J., Blackburn, H.M., 2005. Three-dimensional instabilities and transition of steady and pulsatile axisymmetric stenotic flows. J. Fluid Mech. 533, 297–327.

Stroka, K.M., Hayenga, H.N., Aranda-Espinoza, H., 2013. Human neutrophil cytoskeletal dynamics and contractility actively contribute to trans-endothelial migration. PLoS ONE 8 (4), e61377. https://doi.org/10.1371/journal.pone.0061377.

Timmins, L.H., Molony, D.S., Eshtehardi, P., McDaniel, M.C., Oshinski, J.N., Samady, H., Giddens, D.P., 2015. Focal association between wall shear stress and clinical coronary artery disease progression. Ann. Biomed. Eng. 43 (1), 94–106. https://doi.org/10.1007/s10439-014-1155-9. PubMed PMID: 25316593.

Ting, H.J., Stice, P.J., Schaff, U.Y., Hui, D.Y., Rutledge, J.C., Knowlton, A.A., Passerini, A.G., Simon, S.I., 2007. Triglyceride-rich lipoproteins prime aortic endothelium for an enhanced inflammatory response to tumor necrosis factor-alpha. Circ. Res. 100 (3), 381–390.

Varghese, S.S., Frankel, S.H., Fischer, P.F., 2007a. Direct numerical simulation of stenotic flows. Part 1. Steady flow. J. Fluid Mech. 582, 253–280.

Varghese, S.S., Frankel, S.H., Fischer, P.F., 2007b. Direct numerical simulation of stenotic flows. Part 2. Pulsatile flow. J. Fluid Mech. 582, 281–318.